Structure and Function of a Human $TAF_{II}250$ Double Bromodomain Module

Raymond H. Jacobson, Andreas G. Ladurner, David S. King, Robert Tjian*

TFIID is a large multiprotein complex that initiates assembly of the transcription machinery. It is unclear how TFIID recognizes promoters in vivo when templates are nucleosome-bound. Here, it is shown that $TAF_{II}250$, the largest subunit of TFIID, contains two tandem bromodomain modules that bind selectively to multiply acetylated histone H4 peptides. The 2.1 angstrom crystal structure of the double bromodomain reveals two side-by-side, four-helix bundles with a highly polarized surface charge distribution. Each bundle contains an N^{ε}-acetyllysine binding pocket at its center, which results in a structure ideally suited for recognition of diacetylated histone H4 tails. Thus, TFIID may be targeted to specific chromatin-bound promoters and may play a role in chromatin recognition.

RNA transcription of class II genes in eukaryotes requires the assembly of a very large multiprotein apparatus composed of RNA polymerase II along with a complement of accessory factors (*1*). One important component required for Pol II transcription is TFIID (RNA polymerase II transcription factor D), a multisubunit complex that contains the TATA binding protein (TBP) along with at least eight additional subunits known as TAFs (TBP-associated factors) (*2*). TFIID contains the sequence-specific DNA binding activities necessary for recognition of class II promoters and also functions as a mediator of regulatory signals from many upstream activators (*3*). Until recently most in vitro transcription studies have used naked DNA templates, which has restricted such analyses to examination of direct interactions between TFIID, other basal factors, and DNA. However, in eukaryotic cells the template is wrapped around the nucleosomal histone proteins H2A, H2B, H3, and H4 to form chromatin. This packaging greatly alters the template accessibility by large protein complexes, such as TFIID, required for transcriptional initiation.

Studies of transcription in chromatin-containing systems have suggested that transcriptional activity is correlated with acetylation of specific lysine residues in the NH_2-termini of histone molecules (*4*, *5*). However, the mechanisms underlying the modulation of transcriptional activity by these modifications are not understood at the molecular level. With the discovery that $TAF_{II}250$ contained an intrinsic histone acetyltransferase (HAT) activity (*6*), the possibility arose that the basal machinery could also play an active role in chromatin targeting and/or remodeling. In addition to the HAT domain, $TAF_{II}250$ also contains a tandem pair of ~120-residue motifs known as bromodomains. This motif is present in a variety of proteins including nuclear histone acetyltransferases, kinases, and chromatin remodeling factors (*7*, *8*). A double bromodomain module appears to be an invariant element of TFIID (*9*). Nuclear magnetic resonance (NMR) analysis of a single bromodomain from the p300/CBP-associated factor P/CAF (*10*) suggested a potential role for this motif in binding to peptides containing N^{ε}-acetyllysine residues. Here, we report the crystal structure of the double bromodomain module of human $TAF_{II}250$ (residues 1359 to 1638) and examine the interactions between it and acetylated histone peptides. This region of $TAF_{II}250$ may play a part in nucleosome recognition and may mediate acetylation-dependent increases in transcriptional activity.

Based on primary sequence alignments, a fragment containing the double bromodomain from human $TAF_{II}250$ ($hTAF_{II}250$) was subcloned, expressed, and purified (residues 1359 to 1638; $hTAF_{II}250$-DBD) (Table 1). We assayed $hTAF_{II}250$-DBD for its ability to bind a synthetic peptide corresponding to the fully acetylated form of the first 36 amino acids of the histone H4 NH_2-terminal tail. Histone H4 includes four sites of acetylation, which have been correlated with transcriptional activity (K5, K8, K12, and K16) (*11*). The multiple sites of modification could permit simultaneous binding by the two $TAF_{II}250$ bromodo-

Table 1. Crystallographic data, phasing, and refinement. The $hTAF_{II}250$ double bromodomain was expressed at 30°C from a pET21a construct in *E. coli* strain BL21. The recombinant protein was purified with a Perseptive PorosHQ anion-exchange column followed by fractionation with a Pharmacia Superdex 75 size-exclusion column. Initial crystals were grown by mixing equal volumes of $hTAF_{II}250$-DBD (10 mg/ml) and buffer containing 1.4 M $(NH_4)_2SO_4$ and 100 mM tris-HCl (pH 9.5). Fragments of initial crystal clusters were used to seed new drops at 1.0 M $(NH_4)_2SO_4$ containing 100 mM tris-HCl (pH 9.5). Single crystals in space group $P2_12_12_1$ (a = 48.1 Å, b = 58.1 Å, c = 101.5 Å) were obtained. Crystals of a selenomethionine-containing variant were cryoprotected in 3.0 M $(NH_4)_2SO_4$, 30% (w/v) D-sucrose, 100 mM Tricine (pH 9.0), and MAD data were collected from a single crystal at 100 K with the CCD detector at beamline 5.0.2 of the Advanced Light Source, Lawrence Berkeley National Laboratory. Data were processed and scaled and subsequent phase refinement was carried out with the CCP4 set of crystallographic programs (*21*) using shell scripts generated automatically by the program ELVES (*22*). Selenium positions were located with the program VERIFY (*23*). Six of eight potential selenium sites were identified and used for phasing. MAD phases were generated with MLPHARE (*24*) and improved through solvent flattening and histogram matching by the program DM (*25*). The model was built using O (*26*) and subsequently refined with CNS (*27*) using the MLHL maximum likelihood target function in conjunction with the DM-generated set of density-modified phases as prior experimental phase information. Restrained *B*-factor refinement, anisotropic *B*-factor correction, and a bulk solvent model were used in the refinement. The Protein Data Bank accession code for this protein is 1EQF.

Crystallographic data

Data set	λ (Å)	d_{min} (Å)	Observed reflections	Unique reflections	Completeness (%)	$\langle I \rangle / \langle \sigma_I \rangle$	R_{merge}* (%)
Anomalous peak	0.9801	2.1	122,732	17,084	97.6	17.3	7.9 (34.1)
Inflection point	0.9804	2.2	95,818	14,842	96.4	16.5	7.9 (34.7)
High-energy remote	0.9611	2.3	86,182	12,999	97.1	14.4	8.0 (30.8)
Low-energy remote	1.0000	2.2	93,653	14,886	96.7	16.2	7.3 (25.4)

Phasing and refinement

Overall figure of merit to 2.3 Å	MLPHARE: 0.581	DM: 0.721
R factor to 2.1 Å†	R_{cryst}: 22.4%	R_{free}: 24.9%
RMSD from ideality‡	Bond lengths: 0.006 Å	Bond angles: 1.11°
Ramachandran analysis	Most favored: 94.8%	Additionally allowed: 5.2%

*$R_{merge}(I) = \Sigma|I(i) - \langle I(h)\rangle| / \Sigma\langle I(i)\rangle$ where $I(i)$ is the ith observation of the intensity of the *hkl* reflection and $\langle I \rangle$ is the mean intensity from multiple measurements of the *hkl* reflection. †$R_{cryst}(F) = \Sigma_h|F_{obs}(h) - F_{calc}(h)| / \Sigma_h F_{obs}(h)$ where $F_{obs}(h)$ and $F_{calc}(h)$ are the observed and calculated structure factor amplitudes for the *hkl* reflection. R_{free} is the cross-validated *R* factor calculated with 10% of the data omitted from refinement. ‡RMSD is root mean square deviation.

Howard Hughes Medical Institute and Department of Molecular and Cell Biology, 401 Barker Hall, University of California, Berkeley, CA 94720–3204, USA.

*To whom correspondence should be addressed. E-mail: jmlim@uclink4.berkeley.edu

mains to give a 1:1 complex between the $TAF_{II}250$ module and the acetylated tail. Isothermal titration calorimetry (ITC) was used to measure the stoichiometry and affinity of $TAF_{II}250$-DBD for nonacetylated and fully acetylated (K5, K8, K12, and K16) versions of the H4 peptide (Fig. 1). The fully acetylated peptide bound with an affinity of about 5 μM and a 1:1 stoichiometry, but no detectable binding of the corresponding nonacetylated peptide could be observed [estimated dissociation constant (K_d) > 250 μM]. Thus the binding affinity of $TAF_{II}250$ for acetylated H4 peptide is about 70 times higher than that previously reported for the single bromodomain from P/CAF assayed with a monoacetylated histone H4 NH_2-terminal peptide (*10*).

$hTAF_{II}250$-DBD containing selenomethionine was expressed in *Escherichia coli* and purified. Identity and purity were analyzed by electrospray-ionization mass spectrometry. Crystals containing a single copy of the molecule per asymmetric unit were used for subsequent analysis at 2.1 Å resolution by applying the multiwavelength anomalous dispersion (MAD) method (*12*) (Table 1). Clear density was present for all amino acids between residues 1379 and 1624 of the $TAF_{II}250$ sequence. This "core" region includes all residues within the two bromodomain motifs that had been previously identified by inspection of the primary sequence and corresponds to the portions of the sequence with well-defined secondary and tertiary structure. Residues COOH-terminal to the bromodomain motifs (residues 1625 to 1638) were not visible in the experimental map and presumably are disordered. However, weak electron density for the NH_2-terminal residues upstream of the well-defined core domain structure was present and became more readily apparent after model building and subsequent refinement. The NH_2-terminal three residues of $hTAF_{II}250$-DBD form a fortuitous crystal contact with a symmetry-related molecule in the crystal lattice, inserting into one of the apparent acetyllysine binding pockets. The current model contains 267 residues, a SO_4^{2-} ion, and 166 H_2O molecules with a working *R* factor of 22% and an *R*-free value of 25%. Refinement statistics are summarized in Table 1.

A ribbon representation of $hTAF_{II}250$-DBD is shown in Fig. 2. The core of each bromodomain is made up of a four-helix bundle with the same unusual left-handed topology observed in the NMR structure from the human histone acetyltransferase P/CAF (*10*). This topology consists of four antiparallel α helices (αZ, αA, αB, and αC) (*7*) with a long, well-defined loop connecting helices αZ and αA (ZA loop) and a shorter connection between helices αB and αC (BC loop). The ZA and BC loops of each domain in $hTAF_{II}250$-DBD contribute several residues (domain 1: Phe^{1405}, Val^{1409}, Val^{1414}, Tyr^{1417}, Tyr^{1459}, and Leu^{1466}; domain 2: Phe^{1528}, Val^{1532}, Tyr^{1540}, Tyr^{1582}, and Tyr^{1589}) to form deep hydrophobic pockets at the centers of each of the four-helix bundles. These pockets form the putative acetyllysine binding sites and are located at the ends of the bromodomains opposite the NH_2- and COOH-termini. The $TAF_{II}250$ bromodomains contain one extra helix not present in the P/CAF structure. These linking helices (αL) directly follow helix αC in the primary sequence. A sharp bend is formed between helices αC and αL, placing the linking helix across the ends of helices αB and αC and positioning it to connect to the first helix, αZ, of the second bromodomain.

The two bromodomains within the $TAF_{II}250$ fragment adopt essentially identical three-dimensional structures. A least-squares fit calculated by LSQMAN (*13*) located 117 structurally equivalent α carbons with a resultant agreement between α carbon positions of 0.79 Å root mean square. The region displaying the largest discrepancy between the

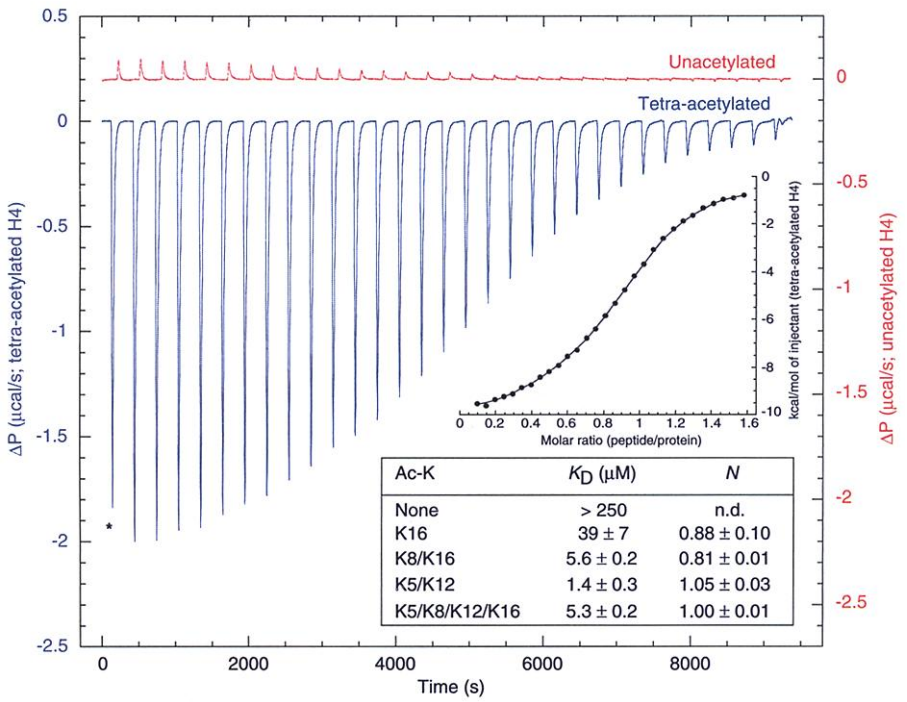

Fig. 1. Isothermal titration calorimetry profiles. Comparison of unacetylated and tetraacetylated peptide binding to the $hTAF_{II}250$ double bromodomain. (Upper left) Differential power (ΔP) data time course for both acetylated and unacetylated peptides corresponding to the first 36 residues of human histone H4. Peptides (~750 μM) were titrated into a solution of $hTAF_{II}250$ double bromodomain (~96 μM). **(Inset)** Calculated affinities and stoichiometries for all H4 peptides tested; Ac-K, positions of acetylation. N^{α}-acetylated histone H4 peptides were synthesized by fluorenyl methoxycarbonyl chemistry on an Applied Biosystems model 431A synthesizer [user-derived dicyclohexyl carbodiimide/1-hydroxybenzotriazole (DCC/HOBT) cycles], cleaved and deprotected with reagent K, and purified by reversed-phase high-pressure liquid chromatography. Peptide purity was assessed by electrospray-ionization ion trap mass spectrometry (Bruker-HP). All peptides contained a mutation of Asp^{25} to Glu to avoid aspartimidyl/isoaspartyl formation and a single nonnative COOH-terminal tyrosine residue to determine peptide concentrations. Experiments were conducted at 25.0° ± 0.1°C with a VP-ITC instrument from MicroCal (Northampton, MA). $hTAF_{II}250$-DBD was dialyzed extensively against 50 mM tris-HCl (pH 7.9), 25 mM NaCl, and 0.25 mM EDTA buffer. Lyophilized peptides were dissolved in the same dialysis buffer. All protein and peptide concentrations were determined by absorbance spectroscopy (Tyr ε_{280}=1,420 M^{-1} cm^{-1}; Trp ε_{280} = 5600 M^{-1} cm^{-}) (*19*).

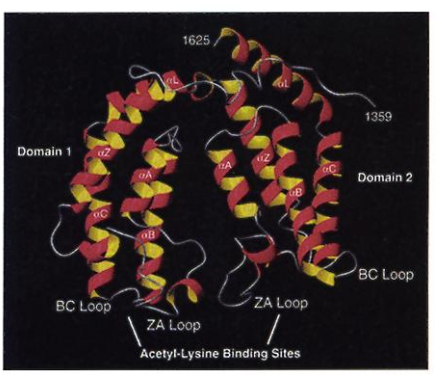

Fig. 2. Ribbon representation of the $hTAF_{II}250$ double bromodomain calculated with Molmol (*20*). Each of the two bromodomains consists of a four-helix bundle with left-handed topology. Linking the helices within the domains are long well-defined ZA loops and shorter BC loops (bottom) responsible for recognition of acetyllysine moieties. The binding pockets are separated by about 25 Å, which makes them ideally positioned to recognize histone tails containing two N^{ε}-acetyllysine residues separated by seven or eight amino acids. The two domains are connected through a linking helix (αL), which is visible running across the top of the domain.

superimposed domains occurs within the αZ helices as a result of an insertion of a single residue in the second domain at position 1518. Although this insertion occurs near the end of helix, it has little effect on the conformation of the ZA loop and is accommodated by a bulge in the αZ helix of the second bromodomain. It is likely that the hydrophobic binding pockets formed from the ZA loops are well conserved among various members of the bromodomain family, which is consistent with a role for these pockets in substrate recognition.

The substrate binding specificity for the double bromodomain would be expected to be tightly coupled to the relative orientation of the two domains and could be enhanced through cooperative binding between the first and second pockets. The relative spatial organization between the two $TAF_{II}250$ bromodomains is given by a 108° rotation about an axis approximately parallel to the principal axes of the four-helix bundles. This arrangement results in a V-shaped structure with the NH_2- and COOH-termini of the fragment close together at one end of the molecule and the two putative acetyllysine binding pockets at the opposite end, separated by about 25 Å.

The interaction interface between the two bromodomains in $hTAF_{II}250$-DBD is composed of two patches separated by a solvent channel. Near the middle of the molecule, glutamate residues 1443, 1444, and 1447 of domain 1 and lysine residues 1555 and 1559 of domain 2 participate in a series of electrostatic interactions. These residues adopt extended conformations that position their side chains in the solvent channel located between the first and second domains, resulting in a pattern of alternating positive and negative charges. At the end of the molecule near the putative binding pockets, the two ZA loops form a complementary hydrophobic interface. This patch is formed from contacts between residues Y1418, K1419, I1420, and T1422 of the first domain and residues P1531, N1533, K1534, K1535, and Y1541 of the second domain (*14*), burying about 160 Å^2 of surface from each. Together the electrostatic and hydrophobic contacts stabilize a conformation that places the binding pockets in a suitable spatial arrangement to recognize a diacetylated peptide with high affinity.

Although the net charge of $TAF_{II}250$-DBD is nearly neutral (predicted pI 6.0), in the three-dimensional structure the charged residues are clustered in distinctly polarized patches. An extended basic patch composed of residues contributed from both of the domains runs diagonally across one of the two largest faces of the double bromodomain module (Fig. 3A). On the opposite side, an equally striking patch of acidic residues runs across the top of the double bromodomain (Fig. 3B). The bottom surface of the molecule contains two deep hydrophobic pockets that are clearly visible (Fig. 3C). The residues that form the extended charged patches are conserved among known metazoan $TAF_{II}250$ sequences, which points to a possible functional role.

A fortuitous crystal contact between symmetry-related molecules within the crystal lattice mimics potential interactions between the bromodomain and acetyllysine residues. The most NH_2-terminal residues of the $TAF_{II}250$ fragment (G1359, T1360, and T1361) are inserted into the hydrophobic pocket from the first domain of a symmetry-related molecule within the crystal lattice. There the first three residues make contact with the conserved aromatic residues F1405, Y1417, and Y1459 and other hydrophobic residues that form the

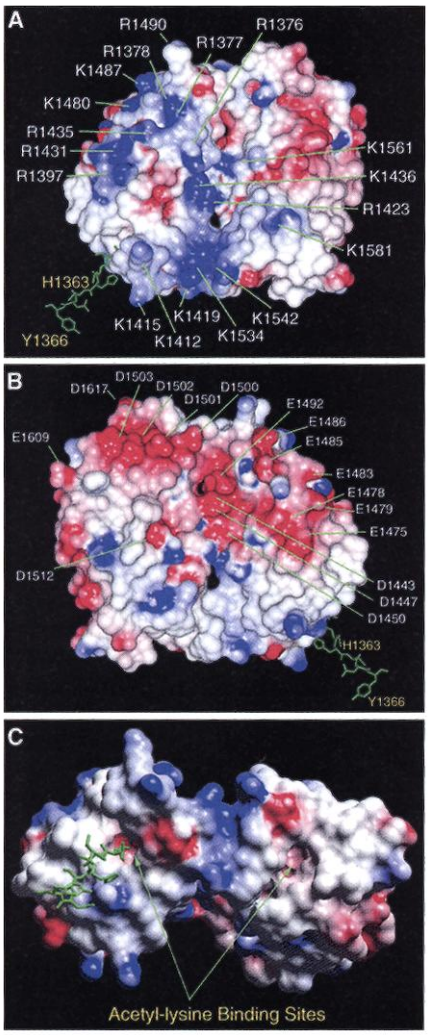

Fig. 3. Electrostatic charge distribution and binding pockets. Delphi electrostatic potential calculated and mapped onto the Connelly solvent accessible surface using InsightII calculated with coordinates corresponding to the core domain (residues 1379 to 1625). Simulated ionic strength was set to 0.145 M with a bulk solvent dielectric constant of 80. The first seven NH_2-terminal residues from a symmetry-equivalent molecule are shown as a green stick model. The first three residues (1359 to 1361) are visible binding into the putative acetyllysine recognition pocket of the first domain. (**A**) Orientation of the $hTAF_{II}250$-DBD is the same as that of Fig. 2. Numerous clustered lysine and arginine residues result in an extended basic surface. (**B**) Reverse side of the double bromodomain relative to (A) displaying the acidic stripe present running across the top of the molecule. (**C**) Putative binding surface of the double bromodomain viewed from the bottom surface of (A). Two deep pits (labeled) at the center of each four-helix bundle are readily apparent and are separated by about 25 Å.

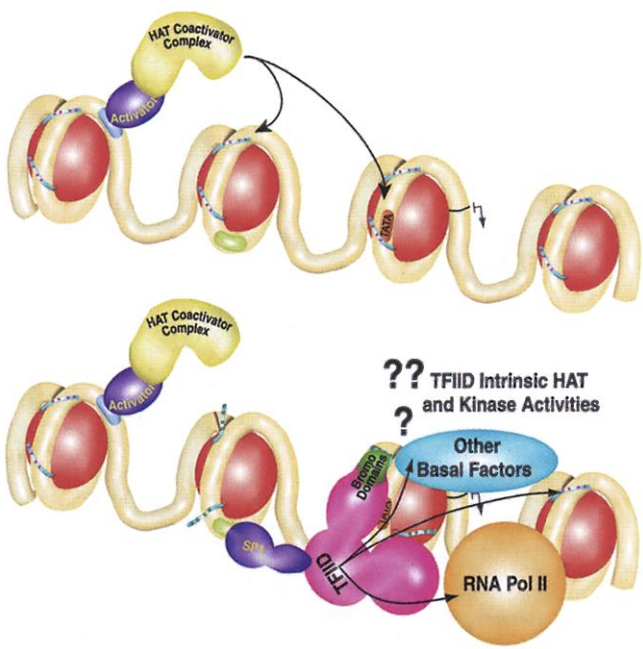

Fig. 4. Simplified model for assembly of transcription complexes on chromatin-bound templates. First, recruitment of a HAT-containing coactivator complex via interactions with an upstream DNA binding protein occurs. After recruitment, the coactivator HAT activity might acetylate the NH_2-terminal histone tails (light blue tails) of nearby nucleosomes (upper). Acetylated histone tails positioned at an appropriate distance from the start site of a gene might then help to recruit TFIID by interactions with the $TAF_{II}250$ bromodomains. Nonspecific interactions between the $TAF_{II}250$ bromodomains and the promoter DNA as well as other TAF-DNA interactions could further increase affinity of TFIID for the core promoter. The bromodomain-mediated increase in affinity for the acetylated histones near the core promoter would provide a linkage between histone acetylation and transcriptional activation by enhanced preinitiation complex formation. Such a model would not preclude other activation pathways.

binding pocket (Fig. 3C).

To span the distance of 25 Å between the two binding pockets would require about seven residues. Sites of acetylation observed on H4 in vivo (K5, K8, K12, and K16) in active euchromatin (*15*) are consistent with this spacing. We performed further binding assays to define which sites of acetylation are important for the $TAF_{II}250$-DBD–H4 interaction. Peptides containing acetyllysine at K16, at K8/K16, and at K5/K12 were synthesized. The ITC measurements (Fig. 1) detected no significant binding for the unacetylated peptide, whereas multiple acetylation of H4 tails at lysine residues K5/K12, K8/K16, or K5/K8/K12/K16 dramatically enhanced binding. The K5/K12 peptide bound most tightly (K_d = 1.4 ± 0.3 μM; n = 1.05 ± 0.03), followed by the K5/K8/K12/K16 peptide (K_d = 5.3 ± 0.2 μM; n = 1.00 ± 0.01). Affinity for the fully acetylated K5/K8/K12/K16 peptide did not dramatically increase relative to K8/K16 (K_d = 5.6 ± 0.2 μM; n = 0.81 ± 0.01). However, singly acetylated peptides (K16) bound with reduced but still significant affinity (K_d ~ 40 μM) (Fig. 1). In contrast, a control peptide (KPGQPMYKGKKALRRQETVDAL) unrelated to histone tails acetylated at the NH_2-terminus and at K8 did not bind detectably to the bromodomains of $TAF_{II}250$. These data suggest that a single acetylated lysine within a peptide unrelated to histone H4 is not sufficient for high-affinity binding to the $TAF_{II}250$ bromodomains.

The ability of the double bromodomain of $TAF_{II}250$ to recognize histone H4 peptide tails containing transcriptionally relevant patterns of acetylation coupled with the striking distribution of charged residues on the protein fragment's surface hints at a new and unexpected role for $TAF_{II}250$. We suggest that these bromodomains may serve to target TFIID to promoters near or within regions of the chromosome that are nucleosome-bound. This would be in contrast to the notion that TFIID nucleates preinitiation complexes at nucleosome-free regions. Upon recognition of the acetylated tails of histone H4, the charged surfaces of the double bromodomain could potentially make nonspecific contacts with the nucleic acid on the basic side of the double bromodomain and contact the core histone molecules along the acidic surface. This notion provides an attractive possibility because TATA elements are often located near or within nucleosomes in vivo (*16*). A simplified scheme linking histone acetylation and core promoter recognition by TFIID (Fig. 4) might include recruitment by upstream activators of coactivator HAT activities such as CBP (*5*, *17*) or Gcn5 (*18*). These HATs could then acetylate appropriate lysine residues of the histones near core promoters thereby increasing affinity for TFIID. At this point there is no evidence that proteins containing both bromodomains and HAT domains concomitantly bind the same substrate. Thus the $TAF_{II}250$ HAT could potentially acetylate histones downstream of the core promoter, other basal transcription factors, or other as yet unidentified protein targets. This could set up a cascade of acetylation events opening the template and rendering it competent for activated transcription. This model would include a direct role for TFIID in targeting transcriptionally relevant patterns of acetylation within the histone tails and could provide a link between HAT activities and enhanced initiation through increased recruitment of TFIID to genes containing multiply acetylated histone tails.

References and Notes

1. G. Orphanides, T. Lagrange, D. Reinberg, *Genes Dev.* **10**, 2657 (1996).
2. J. A. Goodrich and R. Tjian, *Curr. Opin. Cell Biol.* **6**, 403 (1994).
3. S. K. Burley and R. G. Roeder, *Annu. Rev. Biochem.* **65**, 769 (1996); R. Tjian and T. Maniatis, *Cell* **77**, 5 (1994).
4. P. A. Wade and A. P. Wolffe, *Curr. Biol.* **7**, R82 (1997); M. J. Pazin and J. T. Kadonaga, *Cell* **89**, 325 (1997); P. A. Grant *et al.*, *Genes Dev.* **11**, 1640 (1997); V. V. Ogryzko, R. L. Schiltz, V. Russanova, B. H. Howard, Y. Nakatani, *Cell* **87**, 953 (1996); X. J. Yang, V. V. Ogryzko, J. Nishikawa, B. H. Howard, Y. Nakatani, *Nature* **382**, 319 (1996); T. E. Spencer *et al.*, *Nature* **389**, 194 (1997); H. Chen *et al.*, *Cell* **90**, 569 (1997); V. Allfrey, R. Faulkner, A. Mirsky, *Proc. Natl. Acad. Sci. U.S.A.* **51**, 786 (1964); J. E. Brownell and C. D. Allis, *Curr. Opin. Genet. Dev.* **6**, 176 (1996).
5. A. J. Bannister and T. Kouzarides, *Nature* **384**, 641 (1996).
6. C. A. Mizzen *et al.*, *Cell* **87**, 1261 (1996).
7. F. Jeanmougin, J. M. Wurtz, B. Le Douarin, P. Chambon, R. Losson, *Trends Biochem. Sci.* **22**, 151 (1997).
8. S. R. Haynes *et al.*, *Nucleic Acids Res.* **20**, 2603 (1992).
9. O. Matangkasombut, R. M. Buratowski, N. W. Swilling, S. Buratowski, *Genes Dev.* **14**, 951 (2000).
10. C. Dhalluin *et al.*, *Nature* **399**, 491 (1999).
11. C. A. Johnson, L. P. O'Neill, A. Mitchell, B. M. Turner, *Nucleic Acids. Res.* **26**, 994 (1998); M. H. Kuo *et al.*, *Nature* **383**, 269 (1996); S. Y. Roth and C. D. Allis, *Cell* **87**, 5 (1996); R. E. Sobel, R. G. Cook, C. A. Perry, A. T. Annunziato, C. D. Allis, *Proc. Natl. Acad. Sci. U.S.A.* **92**, 1237 (1995); B. M. Turner, *Cell* **75**, 5 (1993).
12. W. A. Hendrickson and C. M. Ogata, *Methods Enzymol.* **276**, 494 (1997).
13. G. Kleywegt, *Acta Crystallogr. D* **53**, 179 (1994).
14. Amino acid residues are abbreviated as follows: A, Ala; C, Cys; D, Asp; E, Glu; F, Phe; G, Gly; H, His; I, Ile; K, Lys; L, Leu; M, Met; N, Asn; P, Pro; Q, Gln; R, Arg; S, Ser; T, Thr; V, Val; W, Trp; Y, Tyr.
15. D. J. Clarke, L. P. O'Neill, B. M. Turner, *Biochem. J.* **294**, 557 (1993).
16. M. Grunstein, *Annu. Rev. Cell Biol.* **6**, 643 (1990).
17. V. V. Ogryzko *et al.*, *Cell* **94**, 35 (1998).
18. J. E. Brownell *et al.*, *Cell* **84**, 843 (1996).
19. S. C. Gill and P. H. von Hippel, *Anal. Biochem.* **182**, 319 (1989).
20. R. Koradi, M. Billeter, K. Wüthrich, *J. Mol. Graph.* **14**, 29, 51 (1996).
21. Collaborative Computational Project, *Acta. Crystallogr. D* **50**, 760 (1994).
22. J. Holton, unpublished program.
23. S. L. Roderick, unpublished program.
24. Z. Otwinowski, in *Isomorphous Replacement and Anomalous Scattering*, W. Wolf, P. R. Evans, A. G. W. Leslie, Eds. (The CCP4 Study Weekend, SERC Daresbury Laboratory, Daresbury, UK, 1991).
25. K. D. Cowtan and P. Main, *Acta Crystallogr. D* **52**, 43 (1996).
26. T. A. Jones, J. Y. Zou, S. W. Cowan, M. Kjeldgaard, *Acta Crystallogr. D* **47**, 110 (1991).
27. A. T. Brunger *et al.*, *Acta Crystallogr. D* **54**, 905 (1998).

28. Supported in part by grants from the National Institutes of Health, The Wellcome Trust, and the Burroughs Wellcome Fund. We thank J. Endrizzi for assistance maintaining our diffraction facilities and offering helpful advice. We thank J. Holton for the use of ELVES, T. Alber and J. Berger for their insights and observations, and T. Earnest and the staff at the Advanced Light Source for their help. We thank T. Handel and her lab for their support, D. Koshland Jr. and S. Marqusee for use of the MCS-ITC instrument, and M. Haggart for DNA sequencing and oligonucleotide synthesis. We thank D. Rio, M. Botchan, and B. W. Matthews for their comments on the manuscript.

2 February 2000; accepted 6 April 2000

Rapid Destruction of Human Cdc25A in Response to DNA Damage

Niels Mailand, Jacob Falck, Claudia Lukas, Randi G. Syljuåsen, Markus Welcker, Jiri Bartek,* Jiri Lukas

To protect genome integrity and ensure survival, eukaryotic cells exposed to genotoxic stress cease proliferating to provide time for DNA repair. Human cells responded to ultraviolet light or ionizing radiation by rapid, ubiquitin- and proteasome-dependent protein degradation of Cdc25A, a phosphatase that is required for progression from G_1 to S phase of the cell cycle. This response involved activated Chk1 protein kinase but not the p53 pathway, and the persisting inhibitory tyrosine phosphorylation of Cdk2 blocked entry into S phase and DNA replication. Overexpression of Cdc25A bypassed this mechanism, leading to enhanced DNA damage and decreased cell survival. These results identify specific degradation of Cdc25A as part of the DNA damage checkpoint mechanism and suggest how Cdc25A overexpression in human cancers might contribute to tumorigenesis.

High-fidelity maintenance of genomic integrity in eukaryotes is ensured by DNA repair and cell cycle checkpoints, surveillance pathways that respond to DNA damage by inhibiting critical cell cycle events (*1*). The key G_1-phase checkpoint in mammalian cells re-